Chemical Geology 525 (2019) 210–217

Contents lists available at ScienceDirect

Chemical Geology

journal homepage: www.elsevier.com/locate/chemgeo

Adsorption of REEs on kaolinite and halloysite: A link to the REE distribution on clays in the weathering crust of granite

Meijun Yang[1], Xiaoliang Liang[1], Lingya Ma[1], Jian Huang[1], Hongping He[1,*], Jianxi Zhu[1]

[a] CAS Key Laboratory of Mineralogy and Metallogeny/Guangdong Provincial Key Laboratory of Mineral Physics and Materials, Guangzhou Institute of Geochemistry, Chinese Academy of Sciences, Guangzhou 510640, PR China
[b] University of Chinese Academy of Sciences, Beijing 100049, PR China
[c] Institutions of Earth Science, Chinese Academy of Sciences, Beijing 100029, PR China

ARTICLE INFO

Editor: Hailiang Dong

Keywords:
Rare earth elements
Weathered crust elution-deposited REE deposit
Kaolinite
Halloysite
Enrichment
Fractionation

ABSTRACT

The clay minerals, kaolinite and halloysite are dominant hosts for rare earth elements (REEs) in the weathered crust elution-deposited REE deposits. However, the accumulation of REEs on kaolinite and halloysite has not been systematically compared. In this study, the adsorption of complete REE series on kaolinite and halloysite was investigated under different pH levels and ionic strengths, which was linked to the enrichment and fractionation of REEs within the clay fraction of a typical weathered crust elution-deposited REE deposit. At low ionic strength, the adsorption of REEs on kaolinite and halloysite increased with increase in pH, with some noticeable fluctuation observed on halloysite at high pH. All the REEs were adsorbed to a similar extent without apparent fractionation, except for the slight enrichment of heavy REEs (HREEs) at high pH. At high ionic strength, REE adsorption exhibited a linear increase with the increase in pH, particularly at high pH, with HREEs being preferentially adsorbed. Compared to halloysite, kaolinite possessed a higher specific surface area (SSA) normalized adsorption capacity towards REEs. These observed adsorption characteristics could possibly explain the distribution of REEs in the clay fraction along the REE deposit. The decrease of ion-exchangeable REE content with depth was significant for kaolinite, while the REE fractionation was ascribed to the selective adsorption of HREEs on both kaolinite and halloysite. The enrichment and fractionation mechanism of REEs on kaolinite and halloysite were also discussed in terms of the surface chemistry and morphology of the clay minerals and the variations of chemical properties across the REE group.

1. Introduction

Rare earth elements (REEs) are a group of chemically similar elements behaving coherently in nature. In a supergene environment, slight variations in physical and chemical properties of REEs cause their fractionation across the group, making them excellent tracers (Quinn et al., 2006). REE fractionation takes place through the dissolution of REE-bearing minerals (Bosia et al., 2016), complexation to organic and inorganic ligands (Davranche et al., 2004; Kawabe et al., 1999), as well as scavenging by minerals via adsorption (Piasecki and Sverjensky, 2008), surface precipitation (Dardenne et al., 2002) and redox reactions (Bau and Koschinsky, 2009). Thus, the fractionation characteristics of REEs not only indicate the water-rock interactions (Worrall and Pearson, 2001), but also reveal the geochemical evolution of environments (e.g., groundwater, oceans and sediments) and the impacts of the anthropogenic disturbances (e.g., contaminant discharge and transport) on these entities (Clift et al., 2005; Welch et al., 2009). The surficial geochemical behaviours of REEs also have metallogenic significance. During the weathering process, REEs dissolved from REE-bearing minerals are adsorbed on to the secondary minerals in the ores (Xu et al., 2017). Such an REE deposit is called a weathered crust elution-deposited REE deposit, commonly found in South China and supplies the bulk of the world's HREE requirement (Bao and Zhao, 2008).

Given their abundance in supergene environment, fine-grained nature, and large surface area, clay minerals exert a key control on the concentration and migration of REEs (Lalonde et al., 2012). In rivers (Su et al., 2017), groundwater (Johannesson and Hendry, 2000), and oceans (Ohta et al., 2009), clay minerals existing as suspended particulate matter (SPM) considerably constrain the transportation of REEs (Le Meur et al., 2016). Clay minerals are also the main hosts for REEs in

* Corresponding author at: CAS Key Laboratory of Mineralogy and Metallogeny/Guangdong Provincial Key Laboratory of Mineral Physics and Materials, Guangzhou Institute of Geochemistry, Chinese Academy of Sciences, Guangzhou 510640, PR China.
E-mail address: hehp@gig.ac.cn (H. He).
[1] a,b,c

https://doi.org/10.1016/j.chemgeo.2019.07.024
Received 23 January 2019; Received in revised form 22 June 2019; Accepted 19 July 2019
Available online 21 July 2019
0009-2541/

both ancient (Wang et al., 2010) and modern sedimentary environments (Dubinin and Sval'nov, 2001), and weathering crust (Bao and Zhao, 2008). Therefore, it is desirable to investigate the reaction mechanism between clay minerals and REEs.

Under natural pH, clay minerals with negative layer charge are effective in the adsorption of REEs through ion exchange, electrostatic attraction, surface complexation and migration into clay structure (Granados-Correa et al., 2013). The adsorption capacity is largely determined by surface structure, composition, and the surface charge of clay minerals (Yusoff et al., 2013). Especially, 2:1 clay minerals, e.g., montmorillonite and illite with both permanent and variable pH-dependent charge in interlayer and external surfaces, respectively, have higher adsorption capacities than 1:1 kaolin-group minerals that primarily adsorb species onto the external surface (Wainipee et al., 2013). However, the points of zero charge (pH_{pzc}) of kaolinite, illite, and montmorillonite are < 3.7, ~2.5, and 7–9, respectively (Hirst et al., 2017). At a pH range of 4–7 in most natural environments, kaolinite and illite are capable of surface complexation of REEs (Kulik et al., 2000; Sinitsyn et al., 2000), compared to montmorillonite with positive charge at the edge sites (Coppin et al., 2002). This possibly accounts for the predominance of kaolinite instead of montmorillonite in the enrichment of REEs in the weathering profile (Bao and Zhao, 2008). Moreover, in bauxites (Monsels and van Bergen, 2017) and soils (Liu et al., 2016), clay minerals are predominantly kaolinite, contributing significantly to the abundances of REEs. These findings substantiate the importance of kaolinite in the enrichment of REEs in supergene systems.

Besides kaolinite, kaolin-group minerals also include dickite, nacrite, and halloysite. Although they are the product of aqueous weathering or hydrothermal alteration of micas and feldspars at low pH conditions, only kaolinite and halloysite are found and often coexist in modern soils and sediments (Cygan and Tazaki, 2014). In weathered granites and bauxites, both kaolinite and halloysite predominantly contribute to REE adsorption (Liu et al., 2013). Kaolinite consists of $AlO_2(OH)_4$ octahedral sheet and SiO_4 tetrahedral sheet with a plate-like morphology. The adjacent sheets are connected by oxygen to form a layer, while the layers are linked by hydrogen bonding. Under favorable geological conditions, driven by the mismatch in oxygen-sharing tetrahedral and octahedral sheets in the layer, the mineral layers wrap to form a tubular halloysite, resulting in an external and internal surface formed on siloxane (Si-O-Si) and gibbsite-like aluminol (Al-OH) groups, respectively (Yuan et al., 2015). For kaolin-group minerals, the adsorption of REEs primarily takes place at negatively charge sites determined by the exposed Si—O and Al—O sites (Cygan and Tazaki, 2014). When compared to kaolinite with plate morphology, the tubular shape of halloysite endows it with a larger surface area, abundant pore structure, and a higher number of surface hydroxyl groups (Yuan et al., 2008). This indicates the difference in adsorption capacity of kaolinite and halloysite towards REEs, and accordingly distinct effects on the enrichment and fractionation of REEs. However, few studies have comprehensively tackled this topic.

Herein, the adsorption characteristics of complete REE series on kaolinite and halloysite were compared as a function of pH and ionic strength, which was correlated with the partition and fractionation patterns of REEs on the mineral surface. The obtained results were also discussed in terms of the chemical properties of REEs and clay mineral surface, and associated with the partitioning characters of ion-exchangeable REEs between kaolinite and halloysite within a weathering profile. This study sheds new light on the important role of kaolin-group minerals in the enrichment and fractionation of REEs in supergene environment.

2. Experimental

2.1. Starting clays

The well-crystallised and fine-grained Kaolinite sample (Kln) was obtained from the Maoming Kaolin Clay Company in Guangdong Province, China. Halloysite sample (Hal), collected from Linfen, Shanxi Province, China, was purified by sedimentation and dried at 120 °C. Both the samples were sieved to 200 mesh size and dried at 80 °C for 24 h, followed by the analyses of X-ray diffraction (XRD) with formamide intercalation (Churchman et al., 1984) for mineral phases, X-ray fluorescence (XRF) for chemical composition, hexamminecobalt (III) chloride method for cation exchange capacity (CEC), and acid-base titration for zeta potentials (Text S1, Tables S1–S2, Figs. S1–S3).

2.2. Batch adsorption experiment

The REE stock solution was obtained after diluting the inductively coupled plasma mass spectrometry (ICP-MS) standard solution (AccuStandard). Batch experiment for REE adsorption on Kln and Hal samples was performed at 25 °C under atmospheric condition. The background electrolyte solution was prepared by dissolving $NaNO_3$ (0.01 or 0.5 mol L^{-1}) with Milli-Q water. The clay suspension was prepared by mixing 300 mg of Kln or Hal with 600 mL of background electrolyte solution, stirred for 1 h, and then divided into separated solution with a volume of 19 mL. The pH was adjusted from 3.0 to 7.5 in 0.5 pH unit increment, using HNO_3 (0.1 mol L^{-1}) and NaOH (0.1 mol L^{-1}) solution. Then the suspensions were stirred for 2 h, monitored by Mettler-Toledo FiveEasy Plus™ pH meter. Subsequently, 1 mL of REE stock solution containing 2 mg L^{-1} of each lanthanide and Y was introduced into the separated clay suspension, resulting in the initial concentration (C_0) of 100 μg L^{-1} for each REE and a solid mass (M) of 475 mg L^{-1}. The resulted suspension (V = 20 mL) was constantly stirred at 200 rpm for 24 h, the predetermined time for achieving adsorption equilibrium. The pH of the suspension was determined before and after the adsorption experiment, and the variation was observed to be < 0.2 units. After adsorption, the clay particles were separated from the solution by centrifugation at 11000 rpm for 30 min. The supernatant produced was diluted with 2% HNO_3 and analyzed for REE concentrations (C_t) on the ICP-MS with a precision better than 5%. The adsorption coefficient (K_d, mL g^{-1}) was calculated according to Eq. (1):

$$K_d = (C_0/C_t - 1)V/M \quad (1)$$

The release of REEs from Kln or Hal was evaluated by allowing the clay mineral to react with the background electrolyte for 3 days without addition of any REEs (Table S3). The amount of REE released from Kln was higher than that from Hal, which, however, was negligible in comparison with the amount of REEs added during the adsorption experiment. The REE retention by the walls of the containers was also checked in the experiments using REE solution (100 μg L^{-1} for each REE) for 24 h equilibration. The decrease in aqueous concentration for each REE was < 2 μg L^{-1}. This suggests that the adsorption of REEs by containers could be ignored. The dissolution of Kln and Hal during REE adsorption was also monitored at pH 3, 3.5 and 4, by analyzing the concentrations of leaching Al and Si in the supernatant with ICP-AES. At low pH, the dissolution of Al and Si from Kln and Hal was very low (Fig. S4). According to previous studies (Carroll and Walther, 1990; Wieland and Stumm, 1992), the dissolution of kaolinite decreased from acid to neutral pH. Thus, the dissolution of Kln and Hal in the pH range of 3–7.5 was negligible. The reacted clay minerals were also characterized by XRD, without obvious variation of mineral phase (Fig. S5).

2.3. Ion-exchangeable REE content in clays from the weathered crust elution-deposited REE deposit

Field samples were collected by core drilling the weathering profile of a typical granite-type weathered crust elution-deposited REE deposit. The core drill (N24°59′5″; E115°50′23.6″) is located in the Huangshe rare earth mining area of Renju town, Meizhou city, Guangdong Province, China. Huangshe plutons are one of the Late Yanshanian granitoids in South China. Its terrain is dominated by low hills, corresponding to the elevations between 300 and 400 m. The sampling drilling core is dominated by a small hill of ~35 m in height relative to the surrounding land with slopes of < 25°, and covered by grassy vegetation and few trees. The climate of the area is East Asian monsoon-influenced subtropical with an annual average temperature about 25 °C and an annual average rainfall of 1500–2000 mm. This provides ideal conditions for chemical weathering.

The studied weathering profile was drilled by using a custom-made double-tube drilling system consisting of a stainless steel outer tube with a diamond drill bit and an inner PVC tube. A long drill core of 78 m for the entire weathering profile was obtained. The profile was divided into four weathering stages according to variations in texture and colour. The parent rock is fine-grained (0.5–2.0 mm in grain size) equigranular tonalite with a thickness of 12 m, consisting of quartz (~5%), plagioclase (~65%), K-feldspar (~4%), hornblende (~15%) and biotite (~10%). Accessory minerals include titanite, ilmenite, magnetite, zircon, allanite, apatite, monazite and xenotime. The saprolite lying above the bedrock forms a layer parallel to the land surface, approximately 22 m in thickness. The saprolite preserves the plutonic microstructure with the exception of oriented cracks (0.1–10 mm). The rock forming minerals are similar to those in the parent rock with minor alteration, consisting of a mixture of clay minerals and Fe-oxyhydroxides localized in cracks and along grain boundaries. With the increase of weathering degree, biotite and feldspar are gradually weathered, while quartz with strong weathering resistance is gradually enriched in the upper part of the weathering profile. At the saprolite contact area, the weathered layer of yellowish- and reddish-brown colour, is 40 m in thickness, and consists of fine-grained quartz (30–40%), feldspar (15–25%) and clay minerals (~50%). However, the texture of this level is porous with weak cohesion. Above this layer, the lateritic horizon about 5 m in thickness has a more reddish colour up to the surface. This horizon consists of quartz (40–50%) and clay minerals (~40%), with small amounts of feldspars and Fe-oxyhydroxides.

The samples analyzed in this study were mainly distributed in the weathered layer with the enrichment of clays and REEs, i.e., 12.6, 14.9, 18.8, 20.6 and 23.4 m below the topsoil. The pH of the field sample was determined using a 10 mL $CaCl_2$ solution (0.01 mol L^{-1}) with 2.0 g field sample (Munira et al., 2018). The clay fraction was separated by following the procedure reported by Wang et al. (2018), and then analyzed for mineral phase and ion-exchangeable REE contents (Text S2). The variation of kaolinite crystallinity along the weathering profile was evaluated using Hinckley index, determined from the (021) and (111) reflections of XRD patterns.

3. Results

3.1. Sorption edge

All 14 lanthanides showed the same qualitative behaviours at different pH and ionic strengths (Table S4). The variation of logK_d as a function of pH was obtained by selecting Pr, Gd, and Lu as the delegates for light REEs (LREEs), middle REEs (MREEs), and HREEs, respectively. At low ionic strength (0.01 mol L^{-1}), the logK_d values on Hal or Kln were nearly comparable at certain pH values. For instance, the logK_d values of Pr, Gd and Lu on Hal was 3.08 ± 0.06 at pH 3.0, and increased to 4.91 ± 0.05 at pH 5.0. However, with further increase of pH to 7.5, the logK_d values displayed some noticeable fluctuation between 4.39 ± 0.05 and 5.17 ± 0.08 (Fig. 1). In contrast to Hal, the logK_d values on Kln exhibit a linear increase with increasing pH over all studied pH range (Fig. S6). Specifically, the logK_d value for Pr, Gd and Lu at pH 3.0 was 2.86 ± 0.05, and gradually reached 4.39 ± 0.03 at pH 7.5. Notably, at both pH 3.0 (the lowest pH) and pH 7.5 (the highest pH), the logK_d values on Hal were identical to those on Kln.

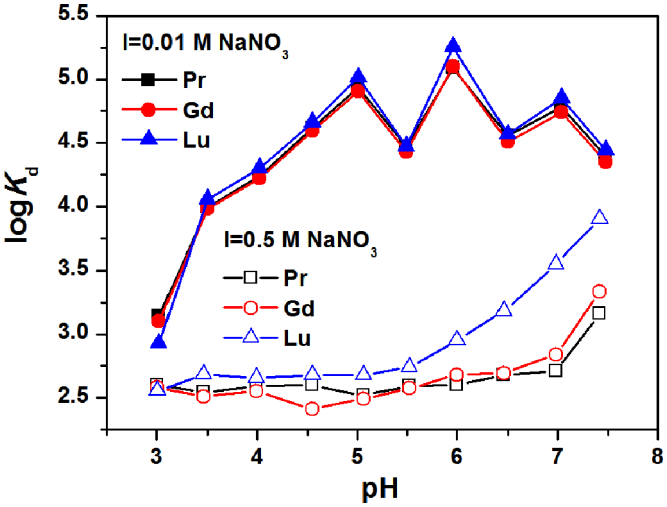

Fig. 1. Logarithm of calculated K_d for Pr, Gd and Lu on Hal as a function of pH at the ionic strengths of 0.01 and 0.5 mol L^{-1}.

At high ionic strength (0.5 mol L^{-1}), the REE adsorption was suppressed, as the logK_d values significantly decreased (Figs. 1 and S6). Moreover, they became distinct fractionated across the REE series, displaying higher log K_d values of HREEs than those of LREEs and MREEs. For example, the logK_d values for Pr, Gd and Lu on Hal remained constant at 2.60 ± 0.10 in the pH range of 3.0–5.0. Above pH 5.0, the logK_d values gradually increased with Lu precedes. At pH 7.5, the logK_d value for Lu on Hal was 3.90, larger than those for Pr (3.33) and Gd (3.16). The adsorption of REEs on Kln at high ionic strength also displayed similar tendency (Fig. S6), but logK_d values of Pr, Gd and Lu were in the range of 0.26–3.04, lower than those on Hal at identical pH.

3.2. Fractionation

The logK_d of Pr, Gd and Lu revealed asynchronous variation with pH, especially at high ionic strength, indicating the occurrence of fractionation across the REE series. In Figs. 2 and S7, the logK_d values obtained for the whole series of lanthanides are plotted as a function of the atomic number. On both Hal and Kln, similar variations of logK_d values with ionic strength were observed. At low ionic strength, the logK_d value was similar throughout the REE series, except Y was slightly less adsorbed than lanthanides. The logK_d ratio of Lu/Pr on both Hal and Kln was close to 1.0 at low pH, but was slightly higher than 1.0 on Kln and Hal in the pH range of 5–6.5 (Fig. 3). The logK_d on Hal was independent of pH, especially in the range of 5.0–7.5 (Fig. 2a), whereas those on Kln showed a significant increase with pH (Fig. S7a). This was consistent with the observations in adsorption edge experiment, where in the pH range of 5–7.5, logK_d displayed noticeable fluctuation on Hal (Fig. 1), but increased with pH on Kln (Fig. S6).

At high ionic strength, due to the extreme suppression of LREE adsorption at low pH (Figs. 1 and S6), the whole pattern of REE adsorption coefficients was only plotted for pH values above 6 for Kln and 5 for Hal. Fractionation was observed across the REE series (Figs. 2b and S7b). In addition to a more obvious Y negative anomaly, the K_d values for both Kln and Hal significantly increased from LREEs to HREEs, which was dependent on pH. For example, the logK_d ratio of

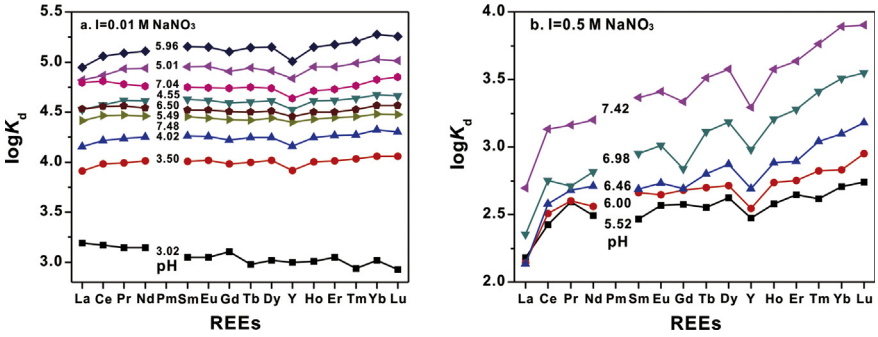

Fig. 2. Plot of logK_d values on Hal as a function of REE atomic number and pH at the ionic strengths of 0.01 (a) and 0.5 (b) mol L^{-1}.

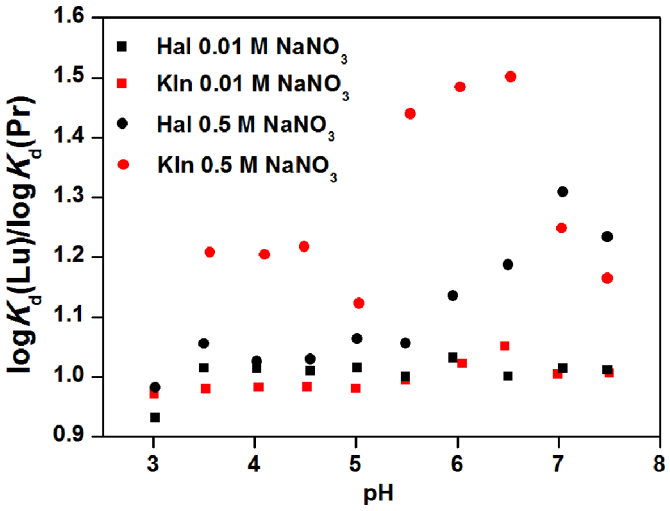

Fig. 3. Variation in logK_d(Lu)/logK_d(Pr) value with pH and ionic strength on Hal and Kln.

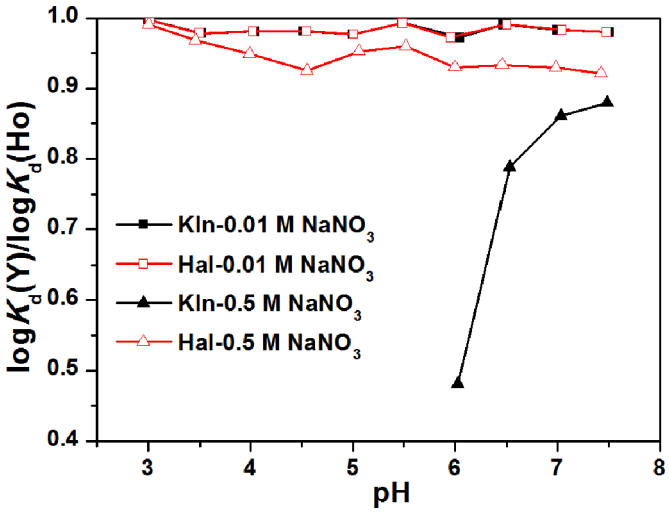

Fig. 4. Variation in logK_d(Y)/logK_d(Ho) value with pH and ionic strength on Hal and Kln.

Lu/Pr on Hal displayed a sudden increase from 1.06 at pH 5 to 1.30 at pH 7, and decreased slightly to 1.24 at pH 7.5 (Fig. 3). Similar but more conspicuous fractionation of REEs was observed on Kln. In the pH range of 5.5–6.5, the logK_d ratio of Lu/Pr on Kln increased from 1.22 to 1.50, and further decreased to 1.16 at pH 7.5. This indicates the enrichment of HREEs on both Hal and Kln at high ionic strength.

Besides REE fractionation, the tetrad effect within the series of La-Nd, Nd-Gd, Gd-Er and Er-Lu was also seen at high ionic strength. Amongst all the elements of the lanthanides series, La and Gd showed apparent negative anomalies, while the negative anomalies of Nd and Er were indistinguishable. Interestingly, with increasing pH, the negative anomalies became progressively less noticeable for Y, La and Gd on Kln (Fig. S7b), but more striking on Hal (Fig. 2b).

Y and Ho are "geochemistry twins" with identical charge and similar ionic radii (Bau, 1999). However, they displayed fractionation, based on the ionic strength and types of clays. At low ionic strength, only slight fractionation appeared on both clay minerals, as the ratio of logK_d(Y)/logK_d(Ho) was close to 1.0 in the studied pH range (Fig. 4). However, fractionation became apparent with increasing ionic strength, notably more on Kln than Hal. At high ionic strength, the value of logK_d(Y)/logK_d(Ho) on Hal was in the range of 0.92–0.99, decreasing with increase in pH value. On the contrary, the ratio of logK_d(Y)/logK_d(Ho) on Kln was much lower, within the range of 0.48–0.88, increasing with increase in pH value.

3.3. Ion-exchangeable REE content of clays from the weathered crust elution-deposited REE deposit

The clay samples separated from the weathered layer for the weathered crust elution-deposited REE deposit, are dominated by kaolinite and halloysite, with a low proportion of illite, montmorillonite or iron (hydr)oxides in certain samples (Table 1, Fig. S9). Such a phase composition of clays is typical in the weathered layer of deposits (Hirst et al., 2017). The proportion of kaolinite and halloysite was determined using XRD with formamide intercalation (Churchman et al., 1984; Joussein et al., 2005). The variation of pH and contents of halloysite, kaolinite and ion-exchangeable REEs along the weathering profile were plotted in Fig. 5. With increase in depth, the pH increased from 5.5 to 6.3, and halloysite content increased from 48% to 81%. In contrast, the kaolinite content dropped from 46% to 19%, with a decrease in crystallinity, as its HI was 1.08, 1.47, 0.52, 0.52 and 0.25 at 12.6, 14.9, 18.8, 20.6 and 23.4 m, respectively. Similar to kaolinite, the ion-exchangeable REE content along the weathering profile layer decreased from 775 ppm to 9 ppm, with an enrichment below the topsoil. The lowest content of REEs appeared in the sample collected at 23.4 m, which displayed the highest content of halloysite (81%) but the lowest

Table 1
Phase composition (wt%) and REE content (ppm) of clay fraction separated from the weathered layer of the weathered crust elution-deposited REE deposit.

Depth/m	Kaolinite	Halloysite	Illite	Other minerals[a]	REE content/ppm
12.6	46	48	3	3	355
14.9	34	51	12	3	775
18.8	44	53	–	3	296
20.6	36	61	–	3	125
23.4	19	81	–	–	9

[a] Other minerals include montmorillonite and iron oxides with content lower than 3%.

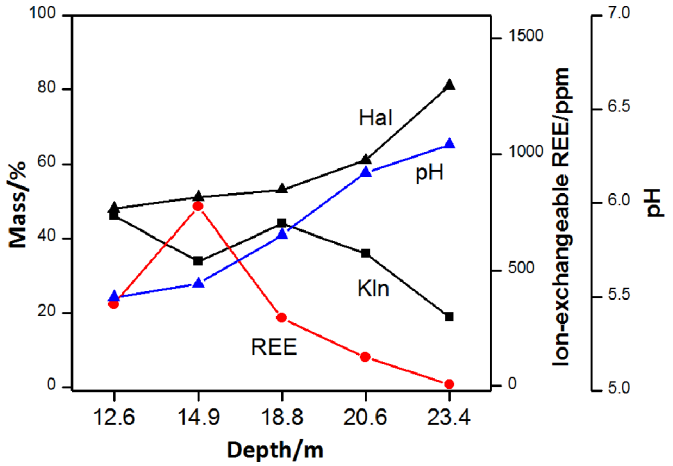

Fig. 5. Variation in contents of pH, ion-exchangeable REEs of clay fraction, kaolinite and halloysite along the weathered layer of the weathered crust elution-deposited REE deposit.

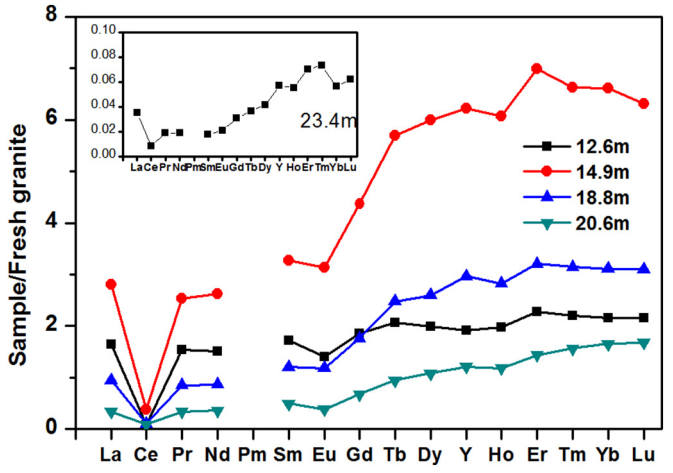

Fig. 6. Fresh granite-normalized patterns of ion-exchangeable REEs on the separated clays along the weathered layer of the weathered crust elution-deposited REE deposit.

content of kaolinite (19%). In terms of REE fractionation, after normalization by the REE contents in fresh granite (Table S5), the ratio of Lu/Pr was 1.40, 2.48, 3.63, 4.95 and 3.29 at 12.6, 14.9, 18.8, 20.6 and 23.4 m, respectively (Fig. 6), indicating the gradual enrichment of HREE. In addition, the negative Ce anomaly gradually decreased along the weathering profile.

4. Discussion

4.1. Sorption edge

Kaolinite and halloysite are the most important members of kaolin-group minerals with a dioctahedral 1:1 layer structure consisting of one tetrahedral and one octahedral sheet. The cations on tetrahedral and octahedral sheets are usually Si^{4+} and Al^{3+}, respectively. The substitution of Si^{4+} with Al^{3+} in the tetrahedral sheets creates a permanent negative charge within the layers. This endows kaolinite and halloysite a certain cation exchange capacity (CEC) (Table S1). Moreover, OH groups at the edges or internal surface/gibbsite basal plane of halloysite and kaolinite are Lewis base or acid functional groups, which are the source of the pH-dependent charge (Strawn and Sparks, 1999). Therefore, the adsorption of REEs on halloysite and kaolinite was constrained by two mechanisms, i.e., pH-independent ion exchange adsorption and pH-dependent surface complexation, whose contributions are affected by pH and ionic strength. From previous study, Eu(III) was adsorbed onto kaolinite mainly by cation exchange below pH 3.5, while inner-sphere complexes started to form at higher pH, as characterized by the adsorption edge experiment combined with time-resolved fluorescence spectroscopy (TRLFS) (Stumpf et al., 2002). In this study, when REEs were adsorbed on Kln and Hal under low ionic strength and pH, ion exchange reaction dominated, where Pr, Gd and Lu displayed similar K_d. However, due to the low CEC of Kln and Hal, i.e., 19.6 and 25.5 meq $(100\,g)^{-1}$, respectively, the exchange reaction could not completely mask the pH-dependent surface complexation, especially at high pH values. Thus, with pH increase, the negative charge on the surface of the clay minerals increased, as shown in the zeta potential curves (Fig. S3). This enriched more REE ions on to the clay surface by forming inner-sphere complexes. Therefore, the $\log K_d$ on Kln linearly increased (estimated slope: 0.33 for Pr, 0.34 for Gd and 0.35 for Lu) (Fig. S6), and the $\log K_d(Lu)/\log K_d(Pr)$ value was slightly higher than 1.0 at high pH range of 5–6.5.

Though the REE adsorption on Hal increased with pH, $\log K_d$ displayed noticeable fluctuation over the pH range of 5.5–7.5 (Fig. 1). Halloysite has a tubular morphology, with the external and internal surfaces being composed of siloxane (Si-O-Si) and aluminol (Al-OH) groups, respectively (Yuan et al., 2015). Compared to the Al-OH groups of halloysite, the affinity of Si-O-Si groups for REEs was subordinate (Tertre et al., 2006), as Eu(III) formed inner-sphere complexes linked to aluminol sites rather than siloxane sites in kaolinite (Ishida et al., 2012). Thus, the internal surface of Hal was a predominant adsorption field for REEs. The adsorption capacity of REEs on Hal and Kln at pH 5 was determined as 3.46 and 1.61 mg g^{-1}, respectively, which was 0.06 and 0.1 mg m^{-2} after the normalization by specific surface area (SSA). Compared to Kln, the normalized adsorption capacity of Hal was lower, which was probably ascribed to the small surface area of the internal surface (Al-OH) in the tubular structure. The adsorption sites on internal hydroxyl surface (Al-OH) are much more than the external siloxane surface. Moreover, over the studied pH range of 3 to 7.5, the halloysite surface was predominantly negative, due to the negative potential of Si-O-Si external surface with a small contribution from the positive Al-OH internal surface. With increase in pH, the surface of Hal became more negatively charged, thereby increasing the electrostatic attraction between positively charged REE ions and negatively charged surface sites, and causing an increase in REE adsorption. However, the solubility of REE hydroxides is very low ($K_{sp} = 10^{-19}$–10^{-24} from La to Lu). Although the REE concentration to solid mass ratio in the experiment was set at a low ratio, with the increase of pH, the formation of fine colloidal hydroxides or surface precipitation would occur. This blocked up the pores of halloysite and inhibited the diffusion of REEs into the lumen of Hal. Thus, the adsorption of REEs at high pH was restrained, resulting in the fluctuation of $\log K_d$. The sorption edge was further quantitatively analyzed by the polynomial fitting of the variation curves of $\log K_d$ with pH (Fig. S8). The highest adsorption for Pr, Gd and Lu appeared at pH 5.8. Then the adsorption showed a decreasing tendency, where the average $\log K_d$ for Pr, Gd and Lu was at 4.6–4.8 in the pH range of 6–7.5. This further verifies that the adsorption of REEs into the lumen of Hal was inhibited. A similar phenomenon was also observed in the adsorption of uranium on halloysite (Kilislioglu and Bilgin, 2002), where the adsorption capacity of uranium increased with the pH increase, achieving the maximum around pH of 3.5. Then the adsorption declined thereafter, ascribed to the clogging of the surface pores by colloidal hydroxides of uranium and the formation of surface precipitation.

At high ionic strength, as the ratio of Na^+/REE^{3+} in the solution became much higher, the exchangeable sites on Hal and Kln were saturated by Na^+. The REE adsorption through ion-exchange reaction was completely inhibited, leading to a significant decrease of $\log K_d$ (Figs. 1 and S6). The REE adsorption was dominated by pH-dependent surface complexation. On one hand, with pH increase, the

deprotonation of variable charge sites enhanced the negative charge on mineral surface and accordingly the electrostatic attraction to REE cations. On the other hand, the deprotonation of variable charge sites also improved the inner-sphere complexation of REEs. Both gave rise to the increase of REE adsorption on Hal and Kln with pH increase (Figs. 1 and S6). Since both Hal and Kln have the same structure unit and chemical composition, their amphoteric sites at the edges were roughly the same. Therefore, they exhibited the same pH-dependent adsorption edge. The hydrated radii of Pr, Gd and Lu were 2.514, 2.405 and 2.307 Å, respectively, decreasing with atomic number (Persson et al., 2008). As REE cations with smaller hydrated radius favored the adsorption, the Lu displayed higher adsorption than Gd and Pr at low ionic strength. The hydrolysis constants (pK1) of Pr, Gd and Lu were 8.32, 7.87 and 7.41, respectively (Yakubovich and Alekseev, 2012). In light of the fact that at high ionic strength, the adsorption of REEs was dominated by inner-sphere complexation, the different hydrolysis ability resulted in the increase of REE adsorption as follows: Pr < Gd < Lu.

4.2. Fractionation

The adsorption of REEs on Hal and Kln displayed distinct fractionation features at different ionic strengths. At low ionic strength, the logK_d values were similar across the REE series on both clay minerals, with the logK_d ratio of Lu/Pr in the range of 1.00–1.05. This was ascribed to the fact that the steric effect of Na^+ was negligible at low ionic strength. All the REEs were adsorbed mainly through cation exchange dominated by electrostatic attraction, resulting in similar adsorption extent. However, adsorption of Y was lower than that of the lanthanides, resulting in a weak negative anomaly (Figs. 2a and S7a). However, as discussed in Section 4.1, partial REEs formed inner-sphere complexes on the surface of Kln and Hal in the pH range of 5–6.5. Thus, the partition pattern of REEs on both Kln and Hal displays slight HREE fractionation. But the adsorption was still dominated by outer-sphere complexation.

At high ionic strength, in addition to the fact that negative anomaly of Y became more evident than that at low ionic strength, the K_d values on both Hal and Kln significantly increased from LREEs to HREEs. The logK_d ratio of Lu/Pr on Hal increased from 1.06 at pH 5 to 1.30 at pH 7, but then decreased to 1.24 at pH 7.5. A similar variation of the logK_d ratio of Lu/Pr was also observed on Kln. As the exchangeable sites on Hal and Kln were saturated by Na^+ at high concentration, the steric constraint inhibited the adsorption of competitors with larger hydrated radii. According to the coordination structure of water-coordinated REE ions, the coordination number decreased with atomic number (Wood, 1990). As a consequence, the adsorption of HREEs with smaller hydrated radii was favored over LREEs with larger hydrated radii. Moreover, under high ionic strength, the adsorption of REEs was predominated by inner-sphere complexation. The decrease in desolvation energy with the atomic number of REEs caused the relative enrichment of HREEs on both clay minerals. The fractionation of REEs was also affected by pH (Figs. 2 and S7). Based on the adsorption edge experiment, REE adsorption was enhanced by pH, which further promoted fractionation. Similar phenomena were also observed in the REE adsorption on montmorillonite at high ionic strength, as reported by Coppin et al. (2002). However, at higher pH of 7.5, the fractionation was inhibited, as evidenced by the decrease of the logK_d ratio of Lu/Pr. This was possibly related to the occurrence of REE precipitation on clay surface (Dong et al., 2012; Piasecki and Sverjensky, 2008).

Previous studies illustrated that at high ionic strength, HREEs are preferentially removed from aqueous solutions by minerals, e.g., kaolinite, montmorillonite and Fe-Mn oxides, without the presence of strong solution complexing ligands, e.g. carbonate and humic acids (Kawabe et al., 1999; Wan and Liu, 2006). But LREEs are preferentially removed by the adsorption from solutions doped with carbonate ions/humic acids, due to the strong complexion between HREEs and aqueous carbonate/humic acids. In this study, the fractionation was not obvious at low ionic strength, but HREE enrichment appeared at high ionic strength. This excludes the interference from the formation of aqueous complexes in REE adsorption on Hal and Kln.

As $NaNO_3$ was used as background electrolyte in this study, the effect of nitrate on the enrichment and fractionation feature of REEs was also discussed. According to previous study (Wood, 1990), the stability constants of nitrate-REE complexes (e.g., $\log\beta_{Ce(III)} = 1.13$, $\log\beta_{Eu(III)} = 1.23$) was much lower than those of carbonate-REE complexes (e.g., $\log\beta_{Ce(III)} = 7.56$, $\log\beta_{Eu(III)} = 8.00$). This indicates the effect of aqueous nitrate on REE adsorption was even much lower than that of carbonate. Thus, the interference of nitrite-REE complexation on REE enrichment and fractionation was also excluded.

Across the REE group, the electron configurations are different, e.g., Y^{3+}: [Kr]4d^0, La^{3+}: [Xe]4f^0, Gd^{3+}: [Xe]4f^7, Lu: [Kr]4f^{14}. As the 4f transition electrons shield the nuclear charge less effectively than electrons in other orbitals, Y^{3+} is less covalent than REEs cations including Ho^{3+} (Mioduski, 1993). Therefore, compared to other REE cations, Y^{3+} was less effectively scavenged by minerals through inner-sphere complexation (Liu et al., 2019). At low ionic strength, as REE adsorption on both Kln and Hal was dominated by ion exchange reaction, REEs along with Y were adsorbed to a similar extent. Thus, no obvious fractionation appeared, especially at low pH. With the increase of pH, the inner-sphere complexes gradually formed on the clay surface, resulting in the less adsorption of Y^{3+} and therefore slight negative anomaly (Figs. 2 and S7). At high ionic strength, REEs and Y^{3+} were bonded to Hal and Kln as inner-sphere complexes. The less covalency of Y^{3+} than REEs contributed to the significant negative anomaly of Y^{3+}. The significant negative anomalies of La and Gd at high ionic strength were also ascribed to their specific electron configurations, which made them less covalent than the adjacent elements (Bau, 1999). This results in the less formation of inner-sphere complexes and thus, negative anomalies.

In the present study, Kln exhibited higher SSA-normalized adsorption capacity towards REEs than Hal. At low ionic strength, the REE adsorption mainly relies on ion exchange reaction, whereas partial REEs form inner-sphere complexes at high pH. The adsorption increased with pH, but displayed conspicuous fluctuation on Hal in the pH range of 5.5–7.5. Across the entire pH range studied, the REE series did not show obvious fractionation, except for the slight enrichment of HREEs at high pH. The increase of ionic strength noticeably inhibited the REE adsorption on both clay minerals. At high ionic strength, the adsorption was dominated by inner-sphere complexation and enhanced with pH increase, but the fractionation appeared with the preferable adsorption of HREEs.

The above results highlight the role of halloysite and kaolinite on the enrichment and fractionation of REEs in various supergene environments, e.g., rivers, oceans, soils and sediments. For example, halloysite and kaolinite coexist in gneissic weathering profiles, developed under a temperate climate in the Leucogia area, NE Greece (Papoulis et al., 2004). During the hydrothermal alteration of monazite (Ce), kaolinite absorbed a large proportion of the released Ce, La, and Nd. Ascribed to the tubular structure of halloysite with small internal surface area, it absorbed relatively fewer amounts of these REEs than kaolinite (Papoulis et al., 2004). Thus, the presence of clay minerals, especially kaolinite, significantly reduced the depletion of REEs. A similar phenomenon was observed in the massive halloysite/kaolinite formation at the karst wall in the Paleozoic limestone from southern Belgium (De Putter et al., 2002). The micro- and nanocrystals of (Ce, Nd) monazite precipitated exclusively on kaolinite flakes, but not on halloysite. This was perhaps due to the difference in the morphology of the two minerals; kaolinite generally forms flat flakes while halloysite forms coiled tubes. Tepe et al. carried out estuarine mixing experiments using glacial-fed river waters and seawater (Tepe and Bau, 2016). Strong variance in REE concentration existed between river water (low salinity) and seawater (high salinity). With fairly low organic content but a high load of clay nanoparticles and colloids, river water showed a

higher concentration of REEs than seawater. The addition of river water to seawater resulted in the remobilization of REEs, especially LREEs, from aggregated clay particles. This was ascribed to the fact that the increase of ionic strength inhibited REE adsorption on most clay minerals, e.g., montmorillonite (Coppin et al., 2002), kaolinite and halloysite, but promoted the fractionation with HREE enrichment, as observed in this study.

4.3. Ion-exchangeable REE content of clays from the weathered crust elution-deposited REE deposit

The results from the adsorption experiment were also linked with the variations in content and fractionation patterns of ion-exchangeable REEs on clay fraction along the weathering profile of REE deposited after elution. The ion-exchangeable REEs in the clay fraction are considered to be bonded to clay mineral surface (Ma and Eggleton, 1999). During the pedogenesis process, REE-bearing minerals are dissolved by acidic groundwater at shallower depths, resulting in the release and migration of REEs (Hirst et al., 2017). With increase in depth, as the soil pH changed from acidic to alkalescent (Fig. 5), the mobility of REEs gradually decreased due to the adsorption by minerals. Halloysite and kaolinite were the main clay minerals in the weathering layer, where the content of halloysite was higher than that of kaolinite. From 12.6 to 14.9 m in the profile, the REE content obviously increased from 355 to 775 ppm. The content of kaolinite decreased from 46% to 34%, while those of halloysite and illite increased from 48% and 3% to 51% and 12%, respectively. The great enrichment of REEs at 14.9 m was probably related to the increase of illite content. The adsorption properties of illite and kaolinite towards REEs were compared in previous study (Alshameri et al., 2019). Compared to kaolinite, illite displayed higher adsorption capacity towards REEs. For example, the SSA-normalized adsorption capacity of illite and kaolinite towards La(III) was 0.18 and 0.05 mg m^{-2} at pH 5, respectively. Then the REE content decreased from 296 to 9 ppm with the increase of depth from 18.8 to 23.4 m, which was positive to the variation of kaolinite content, but opposite to that of halloysite one. Due to the high content of halloysite, it should be an important carrier for REEs. But considering the higher adsorption capacity of kaolinite than halloysite, and the decrease in kaolinite crystallization providing more adsorption sites, the contribution of kaolinite on REE enrichment in this section should be comparable to that of halloysite.

With an increase in depth, the HREE enrichment of ion-exchangeable REEs in the clay fraction gradually increased (Fig. 6). This could be explained by the variations in pH and the crystallinity of kaolinite. For subtropical areas in South China, the ionic strength of soils and groundwater is quite low (ca. 0.01 M) (Harter and Naidu, 2001). At low ionic strength, due to the formation of inner-sphere complexes in the pH range of 5 to 6.5, REEs displayed fractionation on kaolinite and halloysite with preferable adsorption of HREEs. Thus, in the studied weathering profile with a pH range of 5.5 to 6.3, the adsorbed REEs by inner-sphere complexation on kaolinite and halloysite increased with profile depth, resulting in the enrichment of HREEs. Moreover, considering that the crystallinity of kaolinite in the weathering profile is not only much poorer than that used in the adsorption experiment, but also decreased along the profile, kaolinite in the weathered layer should have stronger reactivity towards REEs. This led to the higher enrichment and fractionation of HREE, which increased with profile depth. Therefore, most weathered crust elution-deposited REE deposits are characteristic of HREE enrichment. In comparison with other REEs, Ce (III) is prone to oxidation by Fe and Mn (hydro)oxides. Due to the high Fe and Mn (hydro)oxide content and redox potential at shallow level (Bau and Koschinsky, 2009), most Ce is oxidized and present as CeO_2, giving rise to the negative Ce anomaly on clay fraction. With the increase in depth, the oxidation of Ce decreases, as the Ce(III) ions are mainly adsorbed on halloysite and kaolinite without displaying negative Ce anomaly.

5. Conclusions

In the present study, the adsorption of complete REE series on kaolinite and halloysite has been studied over a wide pH range (3–7.5) and under two different ionic strengths (0.01 and 0.5 mol L^{-1} $NaNO_3$). Under low ionic strength, as the REEs are adsorbed through ion exchange and surface complexation, the sorption capacity of both clays increased with pH, just with slight HREE fractionation at high pH levels. The distinct tubular morphology of halloysite resulted in the fluctuation of adsorption capacity at high pH. At high ionic strength, only inner-sphere complexes formed at the surface of clays. The REE fractionation with HREE enrichment increased with pH increase. Kaolinite had a higher SSA-normalized adsorption capacity than halloysite, while both clays contributed to the fractionation of REEs. These observations are perhaps the main reasons for the distribution of REEs along the profile of a typical weathered crust elution-deposited REE deposit. Though the content of kaolinite decreases with profile depth, the contribution on REE enrichment is comparative to halloysite, due to the high adsorption capacity and poor crystallinity of kaolinite. As pH increases with depth, HREEs are preferentially enriched on the surface of kaolinite and halloysite, identical to the case of REE adsorption at low ionic strength. The obtained results would be beneficial for understanding the role of clay minerals in the enrichment and fractionation of REEs in the supergene environment.

Acknowledgements

This work was financially supported by the National Key R&D Program of China (Grant No. 2017YFC0602306), Science and Technology Program of Guangzhou, China (Grant No. 201804020037), the National Natural Science Foundation of China (Grant Nos. 41773113, 41702041 and 41825003), Youth Innovation Promotion Association CAS, and the Guangdong Special Branch plans (Grant No. 201629015). This is contribution No.IS-2727 from GIGCAS.

Appendix A. Supplementary data

Supplementary information for the REE adsorption results of Kln, as well as the characterization results of XRD, SEM and zeta potential of Kln and halloysite, the dissolution behavior of Kln and Hal, the XRD results for the clay samples separated from weathered crust elution-deposited REE deposit, the ion-exchangeable REE concentration of the separated clays, can be found in the online version at doi:https://doi.org/10.1016/j.chemgeo.2019.07.024.

References

Alshameri, A., Hongping, H., Chen, X., et al., 2019. Understanding the role of natural clay minerals as effective adsorbents and alternative source of rare earth elements: adsorption operative parameters. Hydrometallurgy 185, 149–161.
Bao, Z.W., Zhao, Z.H., 2008. Geochemistry of mineralization with exchangeable REY in the weathering crusts of granitic rocks in South China. Ore Geol. Rev. 33 (3–4), 519–535.
Bau, M., 1999. Scavenging of dissolved yttrium and rare earths by precipitating iron oxyhydroxide: experimental evidence for Ce oxidation, Y-Ho fractionation, and lanthanide tetrad effect. Geochim. Cosmochim. Acta 63 (1), 67–77.
Bau, M., Koschinsky, A., 2009. Oxidative scavenging of cerium on hydrous Fe oxide: evidence from the distribution of rare earth elements and yttrium between Fe oxides and Mn oxides in hydrogenetic ferromanganese crusts. Geochem. J. 43 (1), 37–47.
Bosia, C., Chabaux, F., Pelt, E., et al., 2016. U-Th-Ra variations in Himalayan river sediments (Gandak river, India): weathering fractionation and/or grain-size sorting? Geochim. Cosmochim. Acta 193, 176–196.
Carroll, S.A., Walther, J.V., 1990. Kaolinite dissolution at 25 degrees, 60 degrees, and 80 degrees C. Am. J Sci. 290 (7), 797–810.
Churchman, G.J., Whitton, J.S., Claridge, G.G.C., et al., 1984. Intercalation method using formamide for differentiating halloysite from kaolinite. Clay Clay Miner. 32 (4), 241–248.
Clift, P.D., Draut, A.E., Kelemen, P.B., et al., 2005. Stratigraphic and geochemical evolution of an oceanic arc upper crustal section: the Jurassic Talkeetna Volcanic Formation, south-central Alaska. Geol. Soc. Am. Bull. 117 (7–8), 902–925.
Coppin, F., Berger, G., Bauer, A., et al., 2002. Sorption of lanthanides on smectite and

kaolinite. Chem. Geol. 182 (1), 57–68.
Cygan, R.T., Tazaki, K., 2014. Interactions of kaolin minerals in the environment. Elements 10 (3), 195–200.
Dardenne, K., Schafer, T., Lindqvist-Reis, P., et al., 2002. Low temperature XAFS investigation on the lutetium binding changes during the 2-line ferrihydrite alteration process. Environ. Sci. Technol. 36 (23), 5092–5099.
Davranche, M., Pourret, O., Gruau, G., et al., 2004. Impact of humate complexation on the adsorption of REE onto Fe oxyhydroxide. J. Colloid Interface Sci. 277 (2), 271–279.
De Putter, T., Andre, L., Bernard, A., et al., 2002. Trace element (Th, U, Pb, REE) behaviour in a cryptokarstic halloysite and kaolinite deposit from Southern Belgium: importance of "accessory" mineral formation for radioactive pollutant trapping. Appl. Geochem. 17 (10), 1313–1328.
Dong, Y.H., Liu, Z.J., Chen, L., 2012. Removal of Zn(II) from aqueous solution by natural halloysite nanotubes. J. Radioanal. Nucl. Chem. 292 (1), 435–443.
Dubinin, A.V., Sval'nov, V.N., 2001. Evolution of sedimentation: a study of authigenic and biogenic phases in pelagic sediments of the Southern Basin, Pacific Ocean. Geochem. Int. 39 (4), 356–372.
Granados-Correa, F., Vilchis-Granados, J., Jimenez-Reyes, M., et al., 2013. Adsorption behaviour of La(III) and Eu(III) ions from aqueous solutions by hydroxyapatite: kinetic, isotherm, and thermodynamic studies. J. Chem. 2012, 1–9.
Harter, R.D., Naidu, R., 2001. An assessment of environmental and solution parameter impact on trace-metal sorption by soils. Soil Sci. Soc. Am. J. 65 (3), 597–612.
Hirst, C., Andersson, P.S., Shaw, S., et al., 2017. Characterisation of Fe-bearing particles and colloids in the Lena River basin, NE Russia. Geochim. Cosmochim. Acta 213, 553–573.
Ishida, K., Saito, T., Aoyagi, N., et al., 2012. Surface speciation of Eu^{3+} adsorbed on kaolinite by time-resolved laser fluorescence spectroscopy (TRLFS) and parallel factor analysis (PARAFAC). J. Colloid Interface Sci. 374, 258–266.
Johannesson, K.H., Hendry, M.J., 2000. Rare earth element geochemistry of groundwaters from a thick till and clay-rich aquitard sequence, Saskatchewan, Canada. Geochim. Cosmochim. Acta 64 (9), 1493–1509.
Joussein, E., Petit, S., Churchman, J., et al., 2005. Halloysite clay minerals - a review. Clay Miner. 40 (4), 383–426.
Kawabe, I., Ohta, A., Miura, N., 1999. Distribution coefficients of REE between Fe oxyhydroxide precipitates and NaCl solutions affected by REE-carbonate complexation. Geochem. J. 33 (3), 181–197.
Kilislioglu, A., Bilgin, B., 2002. Adsorption of uranium on halloysite. Radiochim. Acta 90 (3), 155–160.
Kulik, D.A., Aja, S.U., Sinitsyn, V.A., et al., 2000. Acid-base surface chemistry and sorption of some lanthanides on K^+-saturated marblehead illite: II. A multisite-surface complexation modeling. Geochim. Cosmochim. Acta 64 (2), 195–213.
Lalonde, K., Mucci, A., Ouellet, A., et al., 2012. Preservation of organic matter in sediments promoted by iron. Nature 483 (7388), 198–200.
Le Meur, M., Montarges-Pelletier, E., Bauer, A., et al., 2016. Characterization of suspended particulate matter in the Moselle River (Lorraine, France): evolution along the course of the river and in different hydrologic regimes. J. Soils Sediments 16 (5), 1625–1642.
Liu, X.M., Rudnick, R.L., McDonough, W.F., et al., 2013. Influence of chemical weathering on the composition of the continental crust: insights from Li and Nd isotopes in bauxite profiles developed on Columbia River Basalts. Geochim. Cosmochim. Acta 115, 73–91.
Liu, W.J., Liu, C.Q., Brantley, S.L., et al., 2016. Deep weathering along a granite ridgeline in a subtropical climate. Chem. Geol. 427, 17–34.
Liu, X.M., Hardisty, D.S., Lyons, T.W., et al., 2019. Evaluating the fidelity of the cerium paleoredox tracer during variable carbonate diagenesis on the Great Bahamas Bank. Geochim. Cosmochim. Acta 248, 25–42.
Ma, C., Eggleton, R.A., 1999. Cation exchange capacity of kaolinite. Clay Clay Miner. 47 (2), 174–180.
Mioduski, T., 1993. Covalency of Sc(III), Y(III), Ln(III) and An(III) as manifested in the enthalpies of solution of anhydrous rare earth halides. J. Radioanal. Nucl. Chem. Lett. 176 (5), 371–382.
Monsels, D.A., van Bergen, M.J., 2017. Bauxite formation on Proterozoic bedrock of Suriname. J. Geochem. Explor. 180, 71–90.
Munira, S., Farenhorst, A., Akinremi, W., 2018. Phosphate and glyphosate sorption in soils following long-term phosphate applications. Geoderma 313, 146–153.
Ohta, A., Kagi, H., Nomura, M., et al., 2009. Coordination study of rare earth elements on Fe oxyhydroxide and Mn dioxides: part I. Influence of a multi-electron excitation on EXAFS analyses of La, Pr, Nd, and Sm. Am. Mineral. 94 (4), 467–475.
Papoulis, D., Tsolis-Katagas, P., Katagas, C., 2004. Monazite alteration mechanisms and depletion measurements in kaolins. Appl. Clay Sci. 24 (3–4), 271–285.
Persson, I., D'Angelo, P., De Panfilis, S., et al., 2008. Hydration of lanthanoid(III) ions in aqueous solution and crystalline hydrates studied by EXAFS spectroscopy and crystallography: the myth of the "gadolinium break". Chem. Eur. J. 14 (10), 3056–3066.
Piasecki, W., Sverjensky, D.A., 2008. Speciation of adsorbed yttrium and rare earth elements on oxide surfaces. Geochim. Cosmochim. Acta 72 (16), 3964–3979.
Quinn, K.A., Byrne, R.H., Schijf, J., 2006. Sorption of yttrium and rare earth elements by amorphous ferric hydroxide: influence of pH and ionic strength. Mar. Chem. 99 (1–4), 128–150.
Sinitsyn, V.A., Aja, S.U., Kulik, D.A., et al., 2000. Acid-base surface chemistry and sorption of some lanthanides on K^+-saturated marblehead illite: I. Results of an experimental investigation. Geochim. Cosmochim. Acta 64 (2), 185–194.
Strawn, D.G., Sparks, D.L., 1999. The use of XAFS to distinguish between inner- and outer-sphere lead adsorption complexes on montmorillonite. J. Colloid Interface Sci. 216 (2), 257–269.
Stumpf, T., Bauer, A., Coppin, F., et al., 2002. Inner-sphere, outer-sphere and ternary surface complexes: a TRLFS study of the sorption process of Eu(III) onto smectite and kaolinite. Radiochim. Acta 90 (6), 345–349.
Su, N., Yang, S.Y., Guo, Y.L., et al., 2017. Revisit of rare earth element fractionation during chemical weathering and river sediment transport. Geochem. Geophys. Geosyst. 18 (3), 935–955.
Tepe, N., Bau, M., 2016. Behavior of rare earth elements and yttrium during simulation of arctic estuarine mixing between glacial-fed river waters and seawater and the impact of inorganic (nano-)particles. Chem. Geol. 438, 134–145.
Tertre, E., Berger, G., Simoni, E., et al., 2006. Europium retention onto clay minerals from 25 to 150 °C: experimental measurements, spectroscopic features and sorption modelling. Geochim. Cosmochim. Acta 70 (18), 4563–4578.
Wainipee, W., Cuadros, J., Sephton, M.A., et al., 2013. The effects of oil on As(V) adsorption on illite, kaolinite, montmorillonite and chlorite. Geochim. Cosmochim. Acta 121, 487–502.
Wan, Y.X., Liu, C.Q., 2006. The effect of humic acid on the adsorption of REEs on kaolin. Colloids Surf. A 290 (1–3), 112–117.
Wang, Q.F., Deng, J., Liu, X.F., et al., 2010. Discovery of the REE minerals and its geological significance in the Quyang bauxite deposit, West Guangxi, China. J. Asian Earth Sci. 39 (6), 701–712.
Wang, Z.B., Ma, J.L., Li, J., et al., 2018. Fe (hydro) oxide controls Mo isotope fractionation during the weathering of granite. Geochim. Cosmochim. Acta 226, 1–17.
Welch, S.A., Christy, A.G., Isaacson, L., et al., 2009. Mineralogical control of rare earth elements in acid sulfate soils. Geochim. Cosmochim. Acta 73 (1), 44–64.
Wieland, E., Stumm, W., 1992. Dissolution kinetics of kaolinite in acidic aqueous solutions at 25 °C. Geochim. Cosmochim. Acta 56 (9), 3339–3355.
Wood, S.A., 1990. The aqueous geochemistry of the rare-earth elements and Yttrium. 1. Review of available low-temperature data for inorganic complexes and the inorganic REE speciation of natural-waters. Chem. Geol. 82 (1–2), 159–186.
Worrall, F., Pearson, D.G., 2001. Water-rock interaction in an acidic mine discharge as indicated by rare earth element patterns. Geochim. Cosmochim. Acta 65 (18), 3027–3040.
Xu, C., Kynicky, J., Smith, M.P., et al., 2017. Origin of heavy rare earth mineralization in South China. Nat. Commun. 8.
Yakubovich, Y.Y., Alekseev, V.G., 2012. Hydrolysis constants of tervalent lanthanum and lanthanide ions in 0.1 M KNO_3 solution. Russ. J. Inorg. Chem. 57 (6), 911–915.
Yuan, P., Southon, P.D., Liu, Z.W., et al., 2008. Functionalization of halloysite clay nanotubes by grafting with gamma-aminopropyltriethoxysilane. J. Phys. Chem. C 112 (40), 15742–15751.
Yuan, P., Tan, D.Y., Annabi-Bergaya, F., 2015. Properties and applications of halloysite nanotubes: recent research advances and future prospects. Appl. Clay Sci. 112, 75–93.
Yusoff, Z.M., Ngwenya, B.T., Parsons, I., 2013. Mobility and fractionation of REEs during deep weathering of geochemically contrasting granites in a tropical setting, Malaysia. Chem. Geol. 349, 71–86.